Blawert, C.; Sah, S.P.; Liang, J.; Huang, Y.; Hoeche, D.:
Role of sintering and clay particle additions on coating formation during PEO processing of AM50 magnesium alloy
In: Surface & Coatings Technology (2012) Elsevier

DOI: 10.1016/j.surfcoat.2012.10.013

Role of sintering and clay particle additions on coating formation during PEO processing of AM50 magnesium alloy

Carsten Blawert[a,*], Santosh Prasad Sah[b,1], Jun Liang[a,2], Yuanding Huang[a] and Daniel Höche[a]

[a] Helmholtz-Zentrum Geesthacht Zentrum für Material- und Küstenforschung GmbH, Institute of Materials Research, Max-Planck-Str. 1, 21502 Geesthacht, Germany

[b]Division of Materials Chemistry, Faculty of Engineering, Hokkaido University, Sapporo 060-8628, Japan

[1] Present address: GPO Box 8975, EPC 834, Kathmandu, Nepal

[2] Present address: State Key Laboratory of Solid Lubrication, Lanzhou Institute of Chemical Physics, Chinese Academy of Sciences, 18 Tianshui Middle Road, Lanzhou 730000, China

* Corresponding author – Phone: +49 4152 87 1991, Fax: +49 4152 87 1960, e-mail: carsten.blawert@hzg.de

Abstract

In this study sintering of electrochemical conversion products on the surface of AM50 magnesium alloy by the discharges was identified as an essential step in the coating formation in PEO processing. Clay particles were selected as suitable additives because of their relative low melting point and possible reactions with the substrate-electrolyte conversion products. The comparison of coatings formed in electrolytes with and without particles clearly indicates a complete change in the microstructure. In the standard electrolytes the coatings are crystalline while they are amorphous if particles are present though the energy input (process parameters) was more or less the same. Only the presence and incorporation of the particles into the coating has obviously induced a low temperature reactive liquid phase formation process, reaching a coating composition with glass forming ability which is likely due to the fast cooling by the electrolyte. In contrast, the coating formation in standard electrolytes has

to be considered more like a solid phase sintering. However the results clearly indicate that the sintering of reaction/conversion products by the high energy discharges is a very important step in the coating formation and that the sintering by the discharges in PEO processing can be influenced by the use of additives similar to traditional sintering processes.

Keywords: Magnesium, Plasma Electrolytic Oxidation, Phase formation, Sintering

1. Introduction

Plasma electrolytic oxidation (PEO) is a promising novel process to form ceramic-like coatings of thickness ranging from tens to hundreds microns on light metals (Al, Mg and Ti) and their alloys for corrosion protection, wear resistance, biomimetic and thermal barrier properties [1-13]. The process involves generation of a large number of short-lived microdischarges, caused by dielectric breakdown of oxide film at high voltages, on the entire substrate surface. The formation of the hard and highly crystalline coating is promoted by rapid heating and cooling induced by the microdischarges. The coatings contain many characteristic discharge channels, with the channels becoming larger with the time of PEO treatment [14], such that the coatings formed by PEO are essentially porous. The large discharge pores connecting often the inner coating close to the metal/film interface with the oxide surface are potential defects of the coatings [15, 16] thus avoiding or sealing of these discharge channels is essential to improve the corrosion and tribological performance of the coating. However, precise understanding of formation and self-healing or filling of discharge pores is limited.

The first mechanistic study of PEO was carried out by Van et al. [17] in 1977 and they studied basic electrochemistry and characterized the isolated individual discharges by restricting the process to a needle-head of 18 μm in diameter. They estimated dielectric breakdown potential of at least to be 10,000 V cm^{-1}, the duration of sparks to be ~170 μs and the current associated to be ~70 mA. Additionally, they also estimated the energy of

breakdown to be ~3 MJ and the corresponding energy density must be at least 20 MJ mol^{-1}, a sufficient amount of energy to form molten alumina. The process of PEO is complex involving anodic oxidation, dielectric breakdown, gas evolution (hydrogen and oxygen gas in AC process), cathodic breakdown and plasma thermo-chemical reaction [1]. There are different models, like oxide film dielectric breakdown [17], discharge-in-pore model [18] and contact glow electrolysis [19], to explain the process of PEO. According to a dielectric breakdown model, microdischarges appear due to dielectric breakdown of an oxide film under strong electric field. The breakdown is due to the electron avalanche effects induced by electrolyte species incorporated in the anodic film [20]. An essential condition of dielectric breakdown is that the polarizing voltage should increase proportionally with the film thickness in order to maintain a sufficient electric field in it. However, voltage increase becomes sluggish after initial dielectric breakdown. The discharge in barrier oxide film occurs in filamentary mode and the duration of individual filaments is in the order of 10^{-8} s [21]. However, this model cannot explain why voltage increase is slowed after breakdown and the longer discharge life-time which is of the order of ms. Another model, called discharge-in-pore model, considers that microdischarge is caused by discharge of gas in micropores present in the oxide film. The formation of gas phase in the pore is believed to be induced by an initial dielectric breakdown of a barrier layer in the bottom of the micropore. This model can explain the discharge duration of the order of ms that observed by video imaging. However, the diameter of discharge pore estimated from this model is ~100 μm. Therefore, this model cannot explain the actual pore size of ~5-25 μm in the actual PEO coatings [18]. The next model proposed by Yerokhin et al. is based on 'contact glow discharge electrolysis' [22]. This model considers that a gas envelope is developed at oxide-electrolyte interface. Electrons are injected from electrolyte to the gas envelope. The free electrons will participate in a series of reactions with water, resulting into the formation of gaseous products (H_2 and O_2) that would maintain an environment for stable plasma discharge. The temperature of plasma generated in

PEO was estimated several thousand Kelvin from emission spectroscopy [1]. Such plasma will lead to heating, melting and quenching of underlying oxide layer.

To clarify the process of PEO coating growth, Monfort et al. [23] employed sequential anodizing of Al in silicate and phosphate electrolytes. A PEO coating was first formed in a silicate electrolyte and then in the phosphate electrolyte. EPMA analysis showed that silicon was primarily present in the outer region of the coating and phosphorus was primarily in the inner region of the coating. The selective presence of phosphorus at metal/coating interface shows that new coating material is formed in the vicinity of the metal/coating interface by short-circuit paths formed by discharge events. These results show that the growth of PEO coatings is due to repeated breakdown of oxide film. To estimate the actual temperature that coating is exposed to during breakdown, Matykina et al. [24] employed monoclinic zirconia nanoparticles in the electrolyte. They found that zirconia is incorporated mainly into outer part of the coatings and monoclinic zirconia is changed to tetragonal/orthorhombic one. The presence of tetragonal zirconia in PEO coating shows that temperature during PEO formation is at least ~1710 ºC, which is melting temperature of ZrO_2-Al_2O_3 eutectic, to bring out phase transition of monoclinic zirconia to tetragonal zirconia. Regarding the details of a spark discharge, the research work of Dunleavy et al. showed [25] that discharge current peaks reveal many clusters of current peaks at high resolution and current peaks are discrete. The median duration of a discharge is ~52 μs which is similar to that of the filamentary discharge during insulator breakdown [17]. The life-time of a discharge of 0.25-3.5 ms [22] or 35-800 ms [14] that recorded by video imaging is explained as a cascade of discharges, not of a single one, occurring likely at the physical location. The number of discharge per cascade increases as the coatings thicken [26] and severe damage of the coating is caused by such destructive discharges. Thus, in an attempt to form thicker PEO coatings, the damage by destructive discharges is unavoidable.

Recently it is observed that destructive discharges can be turned to 'soft' sparking by employing a selected AC or bipolar PEO condition with higher cathodic to the anodic current ratio in alkaline silicate electrolyte to form a PEO coating with denser intermediate layer [27]. Formation of such a dense intermediate layer is due to specific role of alkaline silicate electrolyte and cathodic current. Alkaline silicate electrolyte promotes weak dielectric discharges that promote healing of breakdown sites [28]. Additionally, the cathodic current produces nanoporous layer at preceding dielectric breakdown sites and such nanoporous layer is highly resistive for further dielectric breakdown. Hence, cathodic breakdown suppresses repeated dielectric breakdown at same sites, a possible way to form rather dense coating [28-30]. However, dense coating formation by 'soft' PEO is highly selective in terms of power supply, electrolyte and substrate so it is not applicable to form protective coatings of desired composition on every substrate. Whatever the process of PEO is micro-arcing or soft sparking, new coating material is developed at metal/coating interface by short-circuit transport of electrolyte species which are evidenced by sequential micro-arcing PEO in silicate and phosphate electrolytes [23] and using ^{18}O as a tracer in soft PEO [31]. However, where and how the new coating material forms may also depend on the processing parameters such as current and voltage as well as the electrolyte. Electrochemical conversion products are most likely the main source for new coating material. They can form at the interface between metal and coating or on the top surface if solubility limits of certain compounds are exceeded in the electrolyte and solid compounds are deposited at the surface. But also compounds forming in the plasma discharges may be deposited on the surfaces after the discharge is stopped. So there are many sources for new material available, but it is the energy of the discharges that forms from the different reaction products the final solid coating.

Often the energy of the discharges, besides the composition of electrolyte used, is determining what phases will be forming in PEO coatings. In silicate based electrolytes, for example, a certain discharge energy level must be exceeded to produce silicate phases in the coating

while at lower discharge energy levels only MgO is forming [10]. This may suggest that melting of the phases is an essential step in the coating formation and only if the energy of the discharges is high enough to reach the melting point of the phase it can be found to a larger extent in the coating.

However, there are several reports on the reinforcement of PEO coatings by particles which are incorporated from the electrolytes [32-38]. All of them are using particles with a relatively high melting point (> 1700°C) and normally partly reactive or inert incorporation of the particles into the coating is observed depending on the melting point of the particles. In this study, a new approach using low melting point clay particles (< 1200°C) is studied. To our knowledge, no one has used low melting point particles to ease the coating formation process and to seal discharge channels by generating a melt of lower viscosity with the ability to fill the discharge channel before solidification starts immediately after the discharge stopped. Furthermore if successful, the study could demonstrate that liquid phase sintering under the extreme high temperature generated by dielectric discharges is an essential step in the PEO coating formation. The present study consequently follows this idea by adding clay particles to the treatment electrolytes which should work as sintering additives promoting the coating formation by reactive liquid phase formation.

2. Experimental details

AM50 magnesium alloy specimens of size 15 mm × 15 mm × 4 mm were prepared from gravity cast ingot material. The composition (mass fraction) of the substrate material was 4.4% ~ 5.5% Al, 0.26% ~ 0.6% Mn, max. 0.22% Zn, max. 0.1% Si, max. 0.002% Fe, max. 0.001% Cu, max. 0.001 % Ni and Mg balance. The specimens were ground successively with 500, 800, 1200 and 2500 grit emery sheets and cleaned with ethanol before the PEO treatment.

The plasma electrolytic oxidation process was carried out using a pulsed DC power source with a pulse ratio of t_{on} : t_{off} = 2 ms : 20 ms. Two electrolyte compositions representing a phosphorus and a silicon based electrolyte were chosen. The use of a silicon-free phosphorus electrolyte allows an easy control of the successful particle incorporation into the coating as there is no other silicon source than the particles available. Treatments in those electrolytes were performed with and without clay particle additions. The corresponding coatings are called PPEO and SiPEO or with clay particle addition PPEO(C) and SiPEO(C) respectively. The silicate-based electrolyte was prepared using Na_2SiO_3 (10.0 g/l) and KOH (1.0 g/l) in distilled water and the phosphate-based electrolyte was constituted with Na_3PO_4 (10.0 g/l) and KOH (1.0 g/l) in distilled water. Particle additions of 6 and 10 g/l of clay particles (Rockwood Nanofil® 116, natural montmorillonite (about 100% bentonite) of average size of 12 µm [46]), were dispersed into these electrolytes to prepare the particle-containing electrolytes as required. All the PEO treatments were performed at a constant current density of 15 mA cm^{-2} for 30 minutes. In all the cases, the temperature of the electrolyte was kept at 10 ± 2˚C by a water cooling system. The details of the treatments are summarised in Tab. 1. All coated specimens were rinsed thoroughly in distilled water and dried in ambient air immediately after the PEO treatment.

The surface morphology of each surface layer was investigated by optical (LM) and scanning electron microscopy (SEM). Image analysis software analySISpro 5.0 was used to measure the number and size of the open and filled pores. Average values taken from 5 SEM images per treatment condition randomly taken from the specimen surface at 200 x magnification. The surface roughness of the coatings was assessed using a Hommel profilometer. The top view specimens were also characterised by X-ray diffraction measurements (XRD) with Cu K_α radiation to determine the phases present in the layers, and a Zeiss Ultra55 SEM equipped with an energy dispersive spectrometer (EDS) was used to determine the elemental composition of the layers. Furthermore the microstructures of the modified surface layers

were investigated on metallographic prepared cross sections of the specimens using a Cambridge stereoscan 200 SEM. From the cross section SEM micrographs the average layer thickness was estimated and compared with results from non-destructive eddy-current measurements (Minitest 2100). Further information about the coating structure of the coatings prepared with 6 g/l clay addition was obtained by transmission electron microscopy (TEM). For the study the TEM specimens were prepared by focused ion beam (FIB) cutting a thin cross section out of the coating (Fig. 1a) reaching from the top surface across the bulk of the coating and the interface towards the substrate (Fig. 1b). The specimen (Fig. 1b) was selected because it shows representative features of the PEO coating and the interface. The thickness of TEM foil is about 200 to 250 nm. TEM observations were preformed on a Philips CM200 transmission electron microscope operating at 200 kV.

3. Results

3.1. Surface morphology

The surface morphology as shown in Fig. 2 reveals distinct differences between treatments with and without particle additions to the electrolyte, but also between the two standard electrolytes. Nevertheless all the surfaces are dominated by the presence of pores and cracks within the coating. Without particles the surface seems to be smoother which is confirmed by R_a roughness values of 3.82 ± 0.18 µm and 1.19 ± 0.05 µm for the phosphorus and silicon based electrolytes respectively. If particles are added the roughness is increasing to 4.52 ± 0.5 µm and 1.80 ± 0.14 µm respectively and the scatter is much larger. With the standard electrolytes a mixture of open and partly filled pores are visible on the surface. They are formed by the discharges of the PEO process. What is visible is the surface side end of the discharge channel reaching down across the coating towards the substrate. The size is most likely related to the energy in the discharge and the coating composition (melting point)

determining the melted coating volume by the discharge. Larger pores and larger melt volume result more often in closed or partly closed pores as cooling of the larger melt volume is slower and the melt can flow back before solidifying, closing or partly closing the discharge channel after the discharge stopped. Thus open pores are pores which have a black centre in the discharge channel indicating that the bottom or end of the discharge channel is not within the depth resolution of the SEM or the visible bottom is clearly below the rest of the surface. In contrast, in filled pores material is visible in the centre of the discharge channel thus being on the same level as the rest of the coating surface or only on a slightly lower level.

The number of pores is lower in the coatings produced with phosphorus electrolyte but the size is with up to 22 µm larger than in the coating produced with silicon based electrolyte. Latter has pores with up to 11 µm in diameter and almost no filled pores (Tab. 2). If particles are added they are clearly visible on the surface of the produced coatings. They are sticking firmly on the surface indicating that the up-take of the particles occurs mainly over the surface. By subsequent discharges they will be melted and integrated into the coating. The comparison of the original powder with an average particle size of 12 µm (Fig. 2a) and the particles identified on the surfaces (Fig. 2 c, d f and g) suggest that the incorporation is selective. The largest particles visible on the surface have a size of around 10 µm, but the majority of particles sticking on the surface is about 1 to 2 µm or smaller. Such a size is still relative large compared to the pore diameter and thus an incorporation of a larger fraction via the open pores is difficult. All particles with a size larger than 10 µm obviously remain in the electrolyte and are not incorporated.

However the use of particles in the electrolytes clearly reduces the number and size of open pores and increases the number and size of filled pores in both coatings, but much more effective for the phosphorus based coating (Tab. 2). In latter most of the discharge channels are filled by what appears to be melted material thus mainly closed pores are visible and interestingly the size of the pores has increased reaching up to 40 µm in diameter. For the

silicon based coating the influence is less. Even though a large number of filled pores is present now, a number of open pores can be identified still. Interestingly, the size of the open pores was reduced while it is slightly increasing for the closed or filled pores (Tab. 2). Overall, the size of closed pores is always larger than the size of open pores (Tab. 2). The reason for that might be the energy provided by the discharges. Small, low energy discharges may not melt all the phases or the melt volume is small and cooling is quick thus the discharge channels can not be closed by the liquid melt before solidifying forming open pores. If a certain size and energy is reached by the discharges the different phases and components of the coating starts to melt and especially the clay additions are responsible for increasing the melt volume by lowering the melting point. Thus the melt pool around the discharge becomes larger and cooling is slower offering increasing time for the melt to flow back in the discharge channel before solidifying. The result is a larger pore diameter as well as the appearance of filled pores. Summarising, these observations may indicate that on the one hand the clay addition changes the melting behaviour of the coatings and on the other hand an easier melting by the discharges if the coatings are produced in phosphorus based electrolytes.

3.2. Layer thickness and morphology

The growth rate of coatings produced in the phosphorus based electrolyte is much faster than in the silicon based one, resulting in PPEO coatings with an average layer thickness of 30 µm compared to a thickness of 15 µm for SiPEO coatings (Fig. 3). Adding particles to the electrolyte has an opposite effect on the growth rate depending on the base electrolyte used. For the PPEO(C) coating the final average thickness is reduced to about 25 µm while it is increased to 20 µm for the SiPEO(C) coating. Interestingly, the bulk of both coatings contain more spherical pores if particles were present in the electrolyte. Those defects are most likely gas inclusions which were entrapped during solidification, indicating a higher liquid fraction during coating formation compared to coatings produced in particle free electrolytes. Looking at the interfaces a different trend can be observed. Here the defect density is reduced.

Especially for the PPEO coating the interface was very porous and could be greatly improved by the particle addition. The interface in the SiPEO coating was mostly free of larger defects and not much improvement was possible. However, these observations are hardly to quantify because of the preparation process, the larger magnification necessary and variations within the distribution of the defects. So it is also very difficult to decide if the discharge channels were influenced by the particle addition because size and visible length is also determined by the location where the channel was cut during metallographic preparation. However the subjective impression suggests that the order regarding size and length of discharge channels in the four coatings is the following: SiPEO > PPEO > SiPEO(C) > PPEO(C). Another feature of all the coatings are larger elongated pore bands which are orientated parallel to the surface. They occur more severe in both of the phosphorous coatings (PPEO and PPEO(C)) but also in the SiPEO coating. Only for the SiPEO(C) the amount seems to be reduced.

3.3. Microstructure, phase and elemental composition

How effective the addition of particles actually was is visible in the XRD pattern obtained from the four coatings (Fig. 4). While the PPEO and SiPEO coatings are crystalline and composed out of $MgO/Mg_3(PO_4)_2$ and MgO/Mg_2SiO_4 respectively, the PPEO(C) and SiPEO(C) coatings appear to be mainly amorphous. Especially the PPEO(C) coating shows no clear crystalline peaks anymore except those from the Mg substrate (X-rays do penetrate the coating) and one tiny peak that may be correlated with the clay powder sticking on the surface. The SiPEO(C) is also amorphous to a large extent, but some remaining crystalline Mg_2SiO_4 and MgO peaks are still visible. Obviously, the results indicate a complete reactive incorporation of the clay particles forming a new amorphous phase. However this phase forms and seems to be stable over a wider range of composition even if no phosphorus is present in the coating. The composition of the near surfaces is given in Tab. 3. When comparing the PPEO and PPEO(C) compositions it is obvious how much particles were actually incorporated into the coating. The Si content in the coating rises from 0 to 15 at% due to the

clay addition only. In the SiPEO coating the Si content still increased from 18 to 23 at% if clay is present in the electrolyte. This is a clear indication that even the uptake of larger particles in the range of several micrometers in diameter is possible using standard electrolytes. An additional control of the uniformity of the coating composition by EDS analysis of 2 μm^2 regions on cross sections close to the surface, in the centre and close to the interface was performed as well. As shown in Fig. 5 there are no larger variations of the main elements (Mg, Si, O, Al and P) in the coating detected. In all specimens Si is slightly enriched close to the surface and Mg conversion products are enriched closer to the interface. This would be consistent with the main material sources e.g. Si coming from the clay particles or the electrolyte in the case of silicon based electrolytes and Mg from the substrate. However, P in the PPEO(C) specimens is more enriched close to the interface indicating that the anodically driven reactions close to the interface between the substrate and the electrolyte penetrating the coating are also important to produce new coating material most likely in the form of $Mg_3(PO_4)_2$. Unfortunately, the oxygen content appears to be too low in comparison to the direct surface analysis assuming that all the analysed metals would be present in the form of oxides and silicates. However, severe charging effects on the cross sections of the coatings required a sputter-coating with Au to prevent the charging, which may have effects on the quantification even if the Au is ignored in the calculation. Therefore the results are only considered as an indicator of the uniformity across the coating without using the quantified data to calculate phase compositions. Nevertheless, the good uniformity across the whole layer suggests that effective mixing and exchange throughout the layer between the different locations of coating material formation occurs.

To finally determine the structure of the layer an additional TEM examination of the cross section through the PPEO(C) coating was performed. Figure 6 shows the TEM micrographs taken from the top of the coating, the centre, interface and substrate as well as the corresponding diffraction pattern. The micrographs are showing that the coating

microstructure is quite homogenous but it contains microporosity (similar to that already observed in the SEM micrographs) and additional a quite large number of nano sized pores ranging from a few up to several hundred nanometres (Fig. 6 a and b). Latter are isolated and spherical suggesting that they might be formed by gas inclusions when the coating solidifies too quickly and the gas is entrapped. The main fraction of the coating in the top and centre region is obviously an amorphous solid phase, as indicated by the diffuse diffraction. However in the micrographs a few nano-sized particles are also visible especially in the centre region. Here the diffraction shows less diffuse rings with some spots possibly indicating the presence of some nano-crystalline phases within the amorphous matrix. The interface (Fig. 6 c) is clearly nano-crystalline showing defined diffraction rings. The diffraction patterns have been identified as nanocrystalline MgO.

However the most interesting feature is the region where the arrow is pointing at. It shows what is supposed to be a melted substrate region underneath the coating and a discharge channel through the interface ending in the centre of the melted substrate region. This would indicate that at least some of the discharges occur between the substrate and the electrolyte across the whole dielectric coating. The magnesium substrate finally reveals the expected typical hexagonal crystalline diffractions patterns of Mg with a zone axis $[2\bar{1}\bar{1}0]$ (Fig. 6 d).

4. Discussion

First of all the results clearly indicate that even the incorporation of larger size particles from the electrolyte is possible during PEO processing. The clay particles used have an average size of 12 μm diameter, which is much larger than the normally used particles in the range of 300 to 400 nm. Even if the incorporation is selective and the majority of particles incorporated via the surface have only a size of 1 – 2 μm the fraction of open pores is relative small compared to the rest of the surface. This has consequences for the uptake mechanism. The relative large particles must hit the open pores directly to be incorporated via the

discharge channel, but the number of open pores is further reduced due to the particle addition. After particle addition only 0.62% of the PPEO(C) surface is covered with open pores having an average size of 10 μm and 0.4% of the SiPEO(C) surface is covered with open pores having an average size of 7 μm (Tab. 2). Thus the fraction which is incorporated via the discharge channels is supposed to be small and the main uptake occurs from the surface. A large number of particles are visible, firmly attached to the surface when they came obviously in contact with molten regions of the surface. Subsequent discharges at the weak points of the coating will provide the energy to melt new regions around the discharges mixing and converting all material close to the discharge into a melt which finally solidifies as new solid coating material. This would also suggest that coating formation occurs throughout the whole layer. There are many possible sources for new material that has to be converted by the discharges into the new solid coating. Depending on the source the location of formation can vary from the interface, to the bulk or to the surface. The main sources which produce new material by the reaction of substrate and electrolyte components are the current driven anodic oxidation, deposition from the plasma discharges, electrochemical conversion (including dissolution and re-deposition if solubility limits of compounds in the electrolyte are exceeded) and high temperature oxidation products, but also external material like particles added to the electrolyte can be incorporated into the coating. The fact that the whole coating is solid independently whether the new material forms at the coating/substrate interface or at the top surface would suggest that the new material is sintered to the solid coating by dielectric discharges across the whole coating layer. If sintering is important the energy input by the discharges and the melting point of the compounds forming should be an important parameter.

Indeed, re-examine our previous studies regarding the influence of final voltage [39] and current density [10] on the coating microstructure and properties it is obvious that the energy of the discharges is an essential parameter which determines the phase composition of the

coating. In the same silicon based electrolyte a certain energy level was required to actually foster the silicate formation. If the energy in the discharges was lower the MgO formation is dominating. This appears to be inconsistent with the melting points of 2826°C for MgO and 1898°C for Mg_2SiO_4 but one has to consider that the whole process occurs in an aqueous solution, thus even low melting point compounds such as Na_2SiO_3 (1089°C) will not form because they are soluble and others like MgO will form via a different process. At 350°C $Mg(OH)_2$ will decompose into MgO and H_2O [40]. This is a temperature that is easily reached by the discharges even at lower current density or lower discharge voltage. Obviously there is still enough energy available to sinter the MgO once it is formed because a solid coating is present. The formation process might be more a solid state sintering process while it is shifting to more liquid phase sintering if Mg_2SiO_4 forms at higher discharge energy. This opens the question what will happen if sintering additives with low melting point are used to ease the sintering of the compounds. The easiest way to check this concept was via a particle addition to the electrolyte as it is known that particles can be quite easily (at least in the laboratory scale) incorporated into PEO coating from the electrolytes, although it was mainly demonstrated for nano-particles so far [32-36, 41-45] and very rarely for micrometer size particles [37].

Such a sintering additive should be available as a powder, stable in water, compatible to the coating (should contain similar elements) and should have a low melting point to be effective as a sintering additive. These requirements are reducing the suitable powders, so that clay particles with a melting point between 1000 and 1200°C came into the focus of the study, with the additional benefit that they are available in large amounts and varieties as filler material for polymer applications. The selected clay powder (Nanofil116 from Southern Clay Products) is a natural montmorillonite (about 100% bentonite) with an average particle size of 12 µm [46]. Montmorillonite is a hydrated sodium-calcium-aluminium-magnesium silicate hydroxide $(Na,Ca)_{0.33}(Al,Mg)_2(Si_4O_{10})(OH)_2{\cdot}nH_2O$ which can contain potassium, iron, and

other cations as common substitutes. Thus, except iron no other critical elements are expected to be introduced to the PEO process by using the Nanofil powder. The effective incorporation of those relatively large particles during PEO processing was checked by excluding any other Si source than the powder using a pure phosphate based electrolyte in comparison to the standard silicon based electrolyte. The final coating composition (Tab. 3) indicates that there is sufficient up-take of the particles to increase the Si content to 15 at% in the PPEO(C) coating and also the content in the SiPEO(C) is higher compared to the standard SiPEO coating. Unfortunately, up to 2 at% iron was also detected in the final coatings and the effects on the corrosion resistance should be checked or clay with lower iron content must be identified and used.

The layer structure or build-up is not changing much due to the particle addition. There is a thin barrier layer at the interface followed by the porous thick top layer. The top layer is crystalline if no particles are added and mainly amorphous if the clay particles were added to the two treatment electrolytes. In latter case also the amorphous top layer region close to the barrier layer appears to have a less number of defects (Fig. 3). The more detailed TEM study of the PPEO(C) coating revealed that under the present experimental conditions, the average thickness of barrier layer near the interface is about 400 nm. This barrier is dense and mainly composed of nanocrystalline MgO, but still it is a mixture of nanocrystalline and amorphous phases. The obtained result is quite similar to previous results [47-49]. Those investigations on PEO of magnesium alloys in silicate phosphate and/or aluminate-containing alkaline electrolytes indicated that, two or three layer structures can typically be observed with a characteristic thin barrier layer of a few hundred nanometers thickness at the substrate/coating interface. Arrabal et al. observed PEO coatings of magnesium alloys prepared in an electrolyte comprising Na_2SiO_3 and $Na_4P_2O_7$.$10H_2O$ [47], and found the presence of an inner barrier lay with a thickness of 200 nm. Their results demonstrated that the inner layer is MgO, which grows at or near the alloy/coating interface by inward transport of oxygen species.

Hwang et al. investigated PEO behavior of AZ91 Mg alloy in the electrolytes with/without potassium fluoride or $KMnO_4$ [48, 49] and they also observed that the oxide layer has two layers. The outer porous layer consists of a mainly amorphous structure and the structure of the inner dense layer is close to nanocrystalline MgO. The amorphous structure of outer layer was considered to be caused by rapid solidification of oxide layer near surface. However in contrast to our results XRD measurement showed only crystalline diffraction pattern.

Looking further at the microstructure the use of clay as a sintering additive for PEO processing was very successful. Already the morphology of the coating in cross section view indicates a change if particles were added (Fig. 3). A much larger number of spherical pores are visible which are typical for entrapped gas in rapidly solidifying melt. They are mainly located along what appears to be discharge channels from the interface towards the surface and from the visual impression those channels are filled with more material compared to standard treatments without particles. These are indications that the addition of clay particles is able to reduce the viscosity of the melt which is produced by the discharges and there is more time for the melt to flow back into the discharge channel after the discharge is stopped. This is also confirmed by the top view surface morphology shown in Fig. 2. Especially for the PPEO(C) coating the open porosity is extremely reduced and in the pores a dense solidified material is visible. The presence of phosphorus reduces obviously the melting point and viscosity further. Furthermore the whole structure of the coating is changing. After clay addition the main fraction of the coatings is amorphous regardless whether the coating was produced in the phosphorus based or in the silicon based electrolyte. The XRD results (Fig. 4) indicate that still a crystalline fraction of Mg_2SiO_4 is present in the case of the SiPEO(C) coating and the combination of high surface roughness, amorphous phase present and missing standards makes it difficult to quantify both fractions for this type of coating. Without this information it is not possible to determine how much Si is in the crystalline and in the amorphous phase. However in the case of the PPEO(C) coating a 100% amorphous phase can

be assumed without too much error. In that case the amorphous phase should contain all the analysed elements. In consequence, the possible phases and molar fractions based on the content of the major non-oxygen elements can be estimated from the EDS data. If this is done the molar phase composition of the coating would be 11 $MgO \cdot 3\ Na_2O \cdot 15\ SiO_2 \cdot 3\ P_2O_5 \cdot 2.5\ Al_2O_3$. Please note that for this phase composition the analysed oxygen content is not high enough. This can be explained by some substochiometric oxides, some metallic Mg in the coating or some of the metal elements present in the form of phosphates instead of oxides. However, even if the result is not fully consistent as some oxygen is missing it is interesting to see how close the composition is to other glasses (Tab. 4). It is obvious that the coating is far away from standard industrial glasses, but it is within the range of typical bio-glasses. The only major difference is the missing of CaO, but that can be compensated by the higher amount of MgO. So not only the necessary high cooling rates are available (quenching of the melt by the electrolyte after arcing stops), but also the composition of the coating is modified in a way that it melts easier and has a composition close to bio-glasses. Considering this it is not a surprise anymore that the bulk of the coating is composed entirely from an amorphous phase (Fig. 6a and 6b). The results of the SiPEO(C) coating indicates that an amorphisation of major regions of the coating is even possible if there is no phosphorus present in the coating, which may help to further reduce the melting point and improve the glass forming ability.

The presence of the amorphous phases if clay particles were added is a clear indication that at least in the discharge region the coating material was completely melted. Without the clay addition the coatings are still crystalline thus it is likely that even in the discharge region not all the material was melted. Only the clay addition which introduces a phase with low melting point to the process promotes a transition from more solid to liquid phase sintering and together with the change of composition the amorphous solidification is supported. The incorporation of the clay particles occurs fully reactive as in the bulk of the coating no evidence of residual particles is found (Fig. 3 and Fig. 6). As shown in Tab. 1 the processing

conditions are not changing too much if particles are added. For the silicon based electrolytes there is no difference in the processing observed and the final voltages are the same, thus the overall energy input is the same. Only for the phosphorus based electrolyte a slight increase in the final voltage is observed. This might be related to the fact that the PPEO(C) coating is less porous and that a slight increase of 12 V is necessary in the applied constant current operation mode to maintain the same selected current density in comparison to the PPEO coating. However, the life time of the discharges is so short that there was no possibility to determine the real number of discharges to estimate the energy in a single discharge, but from the subjective optical impression also no change occurs. Thus the only difference is the clay which obviously works very well as a sintering additive. Quite a large number of different metallic, organic and inorganic particles were already added to various electrolytes [32-38, 41-45], but they were either different in nature (organic and metallic) or they had quite high melting temperatures. Thus the majority of the powders were either incorporated inert or partly reactive into the coating. In latter case a certain fraction is normally not reacting and the other fraction formed a new crystalline phase by reaction with the substrate, electrolyte components or both of them. This indicates that the process is rather slow and does not take place via a complete melting and mixing of larger coating volumes. The literature suggests that particles or phases (e.g. TiO_2, Mg_2SiO_4) which have melting temperatures below 2000°C can be at least partly melted by the discharges [39, 44] and a liquid phase assisted sintering may occur. At higher melting temperatures the particles are not or only slightly affected by the discharges and they are mainly inert incorporated (e.g. ZrO_2 and SiC) [41-44]. In contrast the good chemical compatibility (same material class) and low melting temperature of the clay allows a complete liquid phase sintering in the discharge region. The whole discharge affected region is melted and good mixing of the whole volume is possible which is indicated by the relatively good homogeneity of the element distribution in the coating (Fig. 5). No crystalline phase remain which may act as a nucleus for crystallisation, the melt composition

is close to bio-glasses and fast cooling by the electrolyte finally allows an amorphous solidification. The fact that the whole coating from the interface to the surface is in an amorphous state implies that the discharges (or at least a fraction from all discharges) are across the whole coating suggesting that at least under the present operating condition they are dielectric discharges. As they affect the whole coating they are also able to convert all the new material into the coating regardless whether it is produced or incorporated on the surface (particles) or close to the interface by reaction of the electrolyte with the substrate. This is supported by the surface incorporation of the relatively large sized clay particles sticking on the surface (Fig. 2) and indications of melted and quenched regions in the substrate close to the interface (Fig. 6c) supposed to be starting and end points of the discharges. The low melting point of the components is responsible for a low viscosity of the melt and good exchange between surface and interface compounds during the life time of a single discharge seen in the good uniformity in the elemental distribution (Fig. 5). Finally the effectiveness of clay particles to promote a complete reactive incorporation of the particles into the coating, creating a single, completely new amorphous phase from all the different compounds present if no clay is added is a clear indicator that sintering is a major process in PEO coating formation. This coating formation can be improved similar to traditional sintering by sintering additives (like clay) which increase the liquid phase fraction and lowers sintering temperatures or improves the speed of sintering.

5. Conclusions

(1) Normally nano-particles (300 – 400 nm) are the preferred choice for particle additions to treatment electrolytes. Present results indicate that even larger particles (with an size of about 10 μm) can be incorporated into PEO coatings on Mg alloy AM50 by additions to the electrolyte.

(2) Sintering seems to be an important step in the coating formation and the available energy in the discharges and the melting points of the compounds in the coating are parameters which determine the phase formation.

(3) Thus the use of "sintering additives" in the form of particle additions to the electrolytes is a new concept to lower the sintering temperatures and improve the coating formation.

(4) The dielectric discharges occur across the whole coating as they are able to convert the particles sticking on the surface as well as the material formed at the interface most likely by anodically driven reaction of dissolved substrate with electrolyte species.

(5) Clay particles are a suitable "sintering additive" because of their stability in aqueous electrolytes, their relative low melting point and their inorganic ceramic nature close to the composition and structure of standard PEO coatings.

(6) With clay particles a complete reactive incorporation of the particles is possible from phosphorous and silicon based electrolytes resulting in uniform coating compositions which are close to commercial bio glasses. The main phase of those coatings is a single amorphous phase.

(7) The combination of the phosphorus based electrolyte and clay particles results obviously in a lower viscosity of the melted volume which allows the melt to flow back into the discharge channel after the discharge turned off. As a consequence more closed porosity is visible compared to coatings produced in silicon based electrolyte.

References

1. A. L. Yerokhin, X. Nie, A. Leyland, A. Matthews, S. J. Dowey, Surf. Coat. Technol. 122 (1999) 73.
2. J. Tian, Z.Z. Luo, S.K. Qi, X.J. Sun, Surf. Coat. Technol. 154 (2002) 1.

3. J. A. Curran, T.W. Clyne, Surf. Coat. Technol. 199 (2005) 168.

4. X. T. Sun, Z. H. Jiang, S. G. Xin, Z. P. Yao, Thin Solid Films 471 (2005) 194.

5. T. B. Wei, F. Y. Yan, J. Tian, J. Alloys Compd. 389 (2005) 169.

6. H. P. Duan, K. Q. Du, C. W. Yan, F. H. Wang, Electrochim. Acta 51 (2006) 2898.

7. R. Arrabal, E. Matykina, F. Viejo, P. Skeldon, G.E. Thompson, Corros. Sci. 50 (2008) 1744.

8. P. B. Srinivasan, C. Blawert, W. Dietzel, Mater. Sci. Eng. A 494 (2008) 401.

9. D. Y. Hwang, Y. A. Kim, D. H. Shin, Mater. Trans. 50 (2009) 671.

10. P. B. Srinivasan, J. Liang, C. Blawert, M. Störmer, W. Dietzel, Appl. Surf. Sci. 255 (2009) 4212.

11. H. A. Chen, G. H. Lv, G. L. Zhang, H. Pang, X. Q. Wang, H. Lee, S. Z. Yang, Surf. Coat. Technol. 205 (2010) S32.

12. W. H. Song, Y. K. Jun, Y. Han, S. H. Hong, Biomaterials 25 (2004) 3341.

13. H. Habazaki, T. Onodera, K. Fushimi, H. Konno, K. Toyotake, Surf. Coat. Technol. 201 (2007) 8730.

14. E. Matykina, A. Berkani, P. Skeldon, G.E. Thompson, Electrochim. Acta 53 (2007) 1987.

15. C. Blawert, V. Heitmann, W. Dietzel, H. M. Nykyforchyn and M. D. Klapkiv, Surf. Coat. Technol. 200 (2005) 68.

16. J. Liang, P. Bala Srinivasan, C. Blawert, W. Dietzel, Electrochim. Acta 55 (2010) 6802.

17. T. B. Van, S.D. Brownand, G. P. Wirtz, Ceramic Bulletin 56 (1977) 563.

18. W. Krysmann, P. Kurze, K.-H. Dittrich and H. G. Schneider, Cryst. Res. Technol. 19 (1984) 973.

19. A. Hickling, M. D. Ingram, Trans. Faraday Soc. 60 (1964) 783.

20. I. Montero, J. M. Albella and J. M. Martinez-Duart, J. Electrochem. Soc. 132 (1985) 814.

21. H.-E. Wagner, R. Brandenburg, K. V. Kozlov, A. Sonnenfeld, P. Michel, J. F. Behnke, Vacuum 71 (2003) 417.

22. A. L. Yerokhin, L. O. Snizhko, N. L. Leyland, A. Pilkington, A. Matthews, J. Phys. D: Appl. Phys. 36 (2003) 2110.

23. F. Monfort, E. Matykina, A. Berkani, P. Skeldon, G. E. Thompson, H. Habazaki, K. Shimizu, Surf. Coat. Technol. 201 (2007) 8671.

24. E. Matykina, R. Arrabal, P. Skeldon, G. E. Thompson, Appl. Surf. Sci. 255 (2008) 2830.

25. C.S. Dunleavy, I.O. Golosnoy, J.A. Curran and T.W. Clyne, Surf. Coat. Technol. 203 (2009) 3410.

26. C.S. Dunleavy, J.A. Curran and T.W. Clyne, Surf. Coat. Technol. 206 (2011) 1051.

27. F. Jaspard-Mercuson, T. Czerwiec, G. Henrion, T. Belmonte, L. Dujardin, A. Viola, J. Beavir, Surf. Coat. Technol. 201 (2007) 8677.

28. S. P. Sah, Y. Tatsuno, Y. Aoki, H. Habazaki, Corros. Sci. 53 (2011)1838.

29. S. P. Sah, E. Tsuji, Y. Aoki, H. Habazaki, Corros. Sci. 55 (2012) 90.

30. S. P. Sah, PhD thesis, Hokkaido University, Japan (2012).

31. E. Matykina, R. Arrabal, D.J. Scurr, A. Baron, P. Skeldon, G.E. Thompson, Corros. Sci. 52 (2010) 1070.

32. J. Guo, L. Wang, S. C. Wang, J. Liang, Q. Xue, F. Yan, J. Mater. Sci. 44 (2009) 1998.

33. M. Aliofkhazraei, A. S. Rouhaghdam, Surf. Coat. Technol. 205 (2010) S51.

34. K. M. Lee, J. O. Jo, E. S. Lee, B. Yoo and D. H. Shin, J. Electrochem. Soc. 158 (2011) C325.

35. Y. L. Song, X. Y. Sun, Y. H. Liu, Mater. Corros. (2011), DOI: 10.1002/maco.201106251.

36. K. M. Lee, K. R. Shin, S. Namgung, B. Yoo, D. H. Shin, Surf. Coat. Technol. 205 (2011) 3779.

37. T. S. Lim, H. S. Ryu, S. -H. Hong, Corros. Sci. 62 (2012) 104.

38. D. Sreekanth, N. Rameshbabu, Mater. Lett. 68 (2012) 439.

39. P.B. Srinivasan, C. Blawert, M. Störmer, W. Dietzel, Surface Engineering, 26 (2010) 340.

40. CRC Handbook of Chemistry and Physics, 78th Ed. (1997), CRC Press, Boca Raton, New York

41. R. Arrabal, E. Matykina, P. Skeldon, G. E. Thompson, Journal of Materials Science 43 (2008) 1532.

42. Yue Yang, Hua Wu, Journal of Materials Science & Technology 26 (2010) 865.

43. R. Arrabal, E. Matykina, F. Viejo, P. Skeldon, G.E. Thompson, M.C. Merino, Applied Surface Science 254 (2008) 6937.

44. K.M. Lee, B.U. Lee, S.I. Yoon, E. S. Lee, B. Yoo, D.H. Shin, Electrochimica Acta 67 (2012) 6.

45. B.S. Necula, L. E. Fratila-Apachitei, A. Berkani, I. Apachitei, J. Duszczyk, J. Mater. Sci: Mater. Med. 20 (2009) 339.

46. Nanofil®116, product bulletin and safety data sheeth, www.scprod.com

47. R. Arrabal, E. Matykina, T. Hashimoto, P. Skeldon, G.E Thompson, Surface and Coatings Technology 203 (2009) 2207.

48. D-Y. Hwang, K-R. Shin, B. Yoo, D-Y. Park, D-H. Shin, D-H. Lee, T Nonferr Metal Soc 19 (2009) 829.

49. D.Y. Hwang, Y.A. Kim, D.H. Shin., Mater Trans 50 (2009) 671.

Tab. 1: Main processing parameters of the four PEO treatments

treatment	treatment time (min)	current density (mA/cm^2)	final voltage (V)
PPEO	30	15	468
PPEO(C)	30	15	480
SiPEO	30	15	460
SiPEO(C)	30	15	460

Tab. 2: Number, size and percentage of the total surface area of open and filled pores determined from image analysis on SEM micrographs at a magnification of 200 x (0.24 mm^2 surface area)

		number of pores	total area of pores (μm^2)	percentage (%)	average pore size (μm^2)	average pore diameter (µm)
	open pores	18 ± 8	2918 ± 2577	1.22	144 ± 63	13 ± 3
PPEO	filled pores	44 ± 11	17305 ± 7535	7.25	410 ± 187	22 ± 5
	open pores	15 ± 7	1490 ± 1278	0.62	89 ± 33	10 ± 2
PPEO(C)	filled pores	21 ± 5	26846 ± 9679	11.25	1297 ± 379	40 ± 6
	open pores	147 ± 5	14584 ± 2631	6.11	99 ± 14	11 ± 1
SiPEO	filled pores	0	-	-	-	-
	open pores	25 ± 6	1097 ± 956	0.4	43 ± 28	10 ± 2
SiPEO(C)	filled pores	47 ± 13	5597 ± 1141	2.35	119 ± 13	12 ± 1

Tab. 3: Surface composition of the four coatings determined by EDS analysis of a larger surface area (1 mm^2)

concentration (at%)	O	Na	Mg	Al	Si	P	C	Fe
PPEO	50	7	27	0	0	12	4	0
PPEO(C)	50	6	11	5	15	6	6	2
SiPEO	47	4	21	1	18	0	10	0
SiPEO(C)	50	4	11	4	23	0	6	2

Tab. 4: Comparison of phase composition of amorphous PPEO(C) coating and commercial bio glasses

Composition (wt%)	Na_2O	MgO	SiO_2	Al_2O_3	P_2O_5	CaO	others
PPEO(C)	8.4	19.9	40.8	11.6	19.3	0	0
Float glass	13.5	3.5	72	1.5	0	8.5	0
Ceravital® bioactive	5-10	2,5-5	40-50		10-15	30-35	0.5-3 K_2O
Biovert I	5.5-9.5	6-28	29.5-50	0-19.5	8-18	13-28	2.5-7 F

Figure captions

Fig. 1: Specimen preparation by FIB a) overview of region from which the specimens were cut and b) selected specimen for TEM analysis

Fig. 2: SEM image of the as received Nanofil 116 clay powder (a) and surface morphology of PEO coatings on AM50 produced either in standard phosphorous based electrolyte b) without and c) with 10 g/l clay particle addition and d) the particles sticking on the surface in higher magnification or in standard silicon based electrolyte e) without and f) with 10 g/l clay particle addition and g) the particles sticking on the surface in higher magnification

Fig. 3: Coating morphology of PEO coatings on AM50 produced either in standard phosphorous based electrolyte a) without and b) with 10 g/l clay particle addition or in standard silicon based electrolyte c) without and d) with 10 g/l clay particle addition

Fig. 4: XRD diffraction pattern of PEO coatings on AM50 produced either in standard phosphorous based electrolyte a) without and b) with 10 g/l clay particle addition or in standard silicon based electrolyte c) without and d) with 10 g/l clay particle addition

Fig. 5: Distribution of the main elements forming the coating measured by EDX small area analysis (2 x 2 μm2) on cross sections about 3 μm from the top surface, in the centre and 3 μm from the interface: a) SiPEO(C) and b) PPEO(C)

Fig. 6: TEM micrographs and corresponding diffraction pattern from various regions of the PPEO(C) coating a) top surface region, b) centre region c) interface region and d) substrate

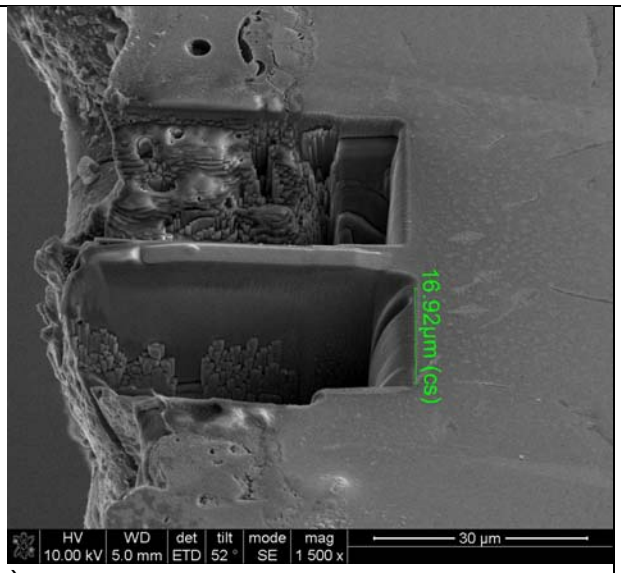
16.92µm (cs)
HV
10.00 kV
WD
5.0 mm
det
ETD
tilt
52 °
mode
SE
mag
1 500 x
30 µm

a)

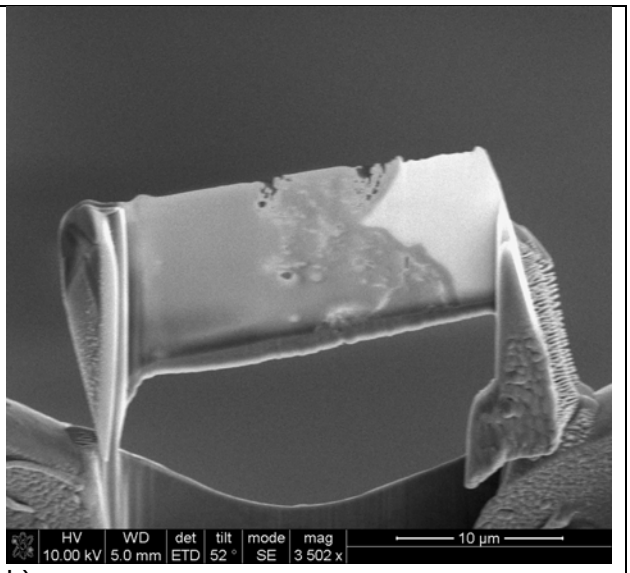
HV
10.00 kV
WD
5.0 mm
det
ETD
tilt
52 °
mode
SE
mag
3 502 x
10 µm

b)

1

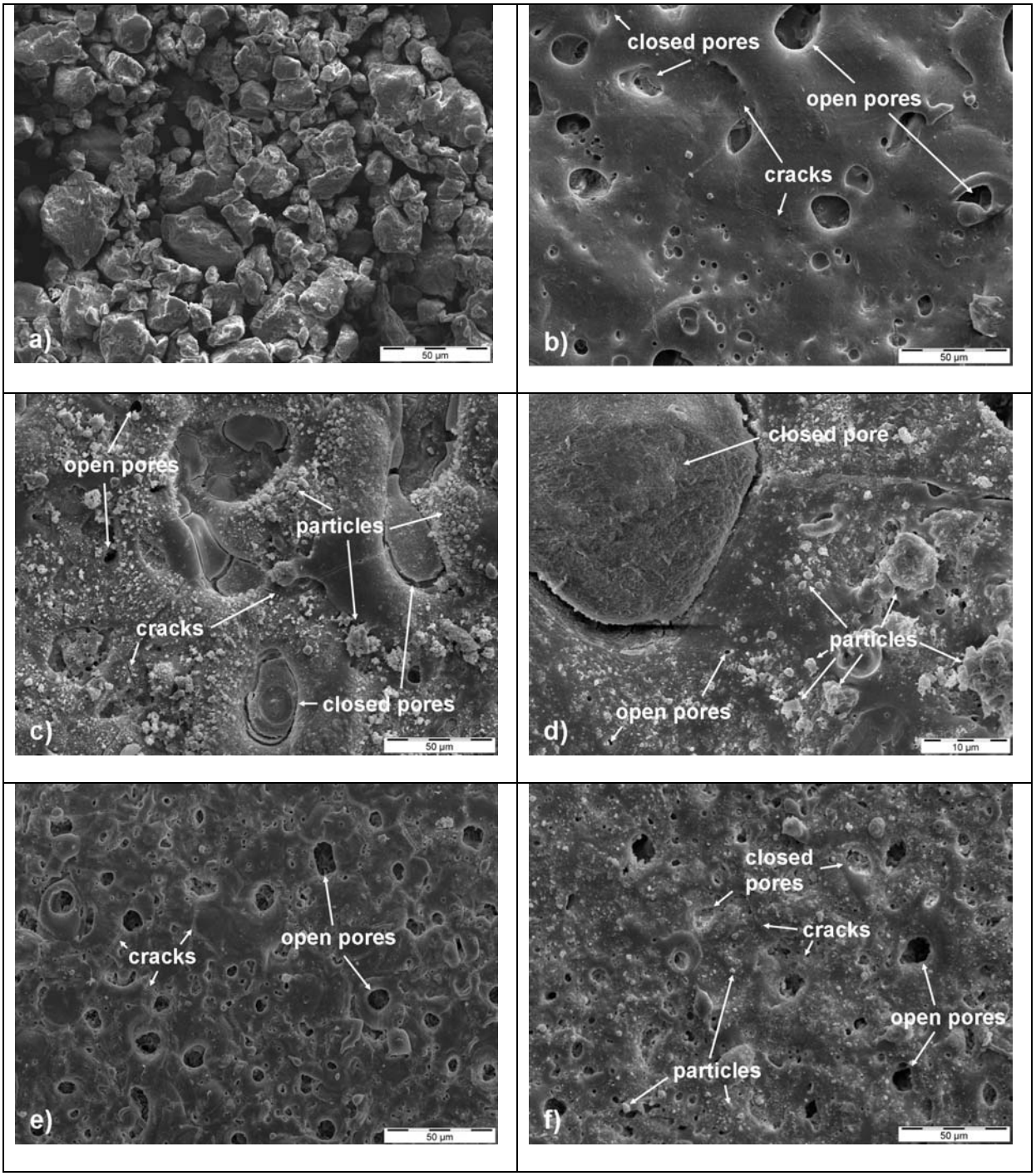
a)
50 µm
closed pores
open pores
cracks
b)
50 µm
open pores
particles
cracks
closed pores
c)
50 µm
closed pore
particles
open pores
d)
10 µm
cracks
open pores
e)
50 µm
closed pores
cracks
open pores
particles
f)
50 µm

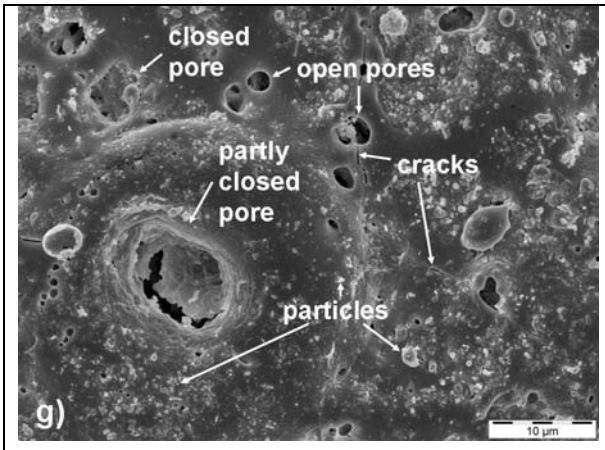
closed
pore
open pores
partly
closed
pore
cracks
particles
g)
10 µm

2

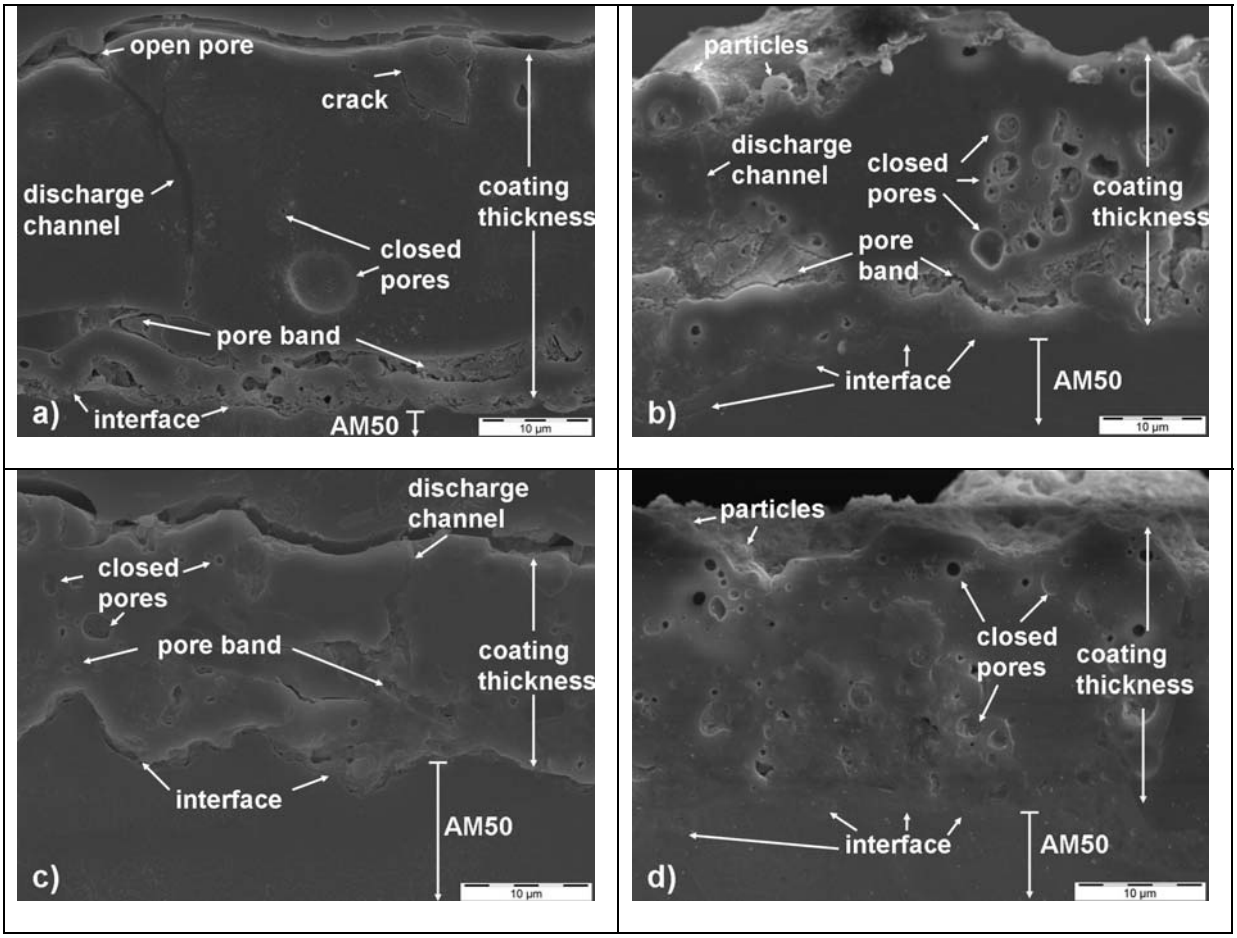
open pore
crack
discharge channel
coating thickness
closed pores
pore band
a)
interface
AM50
10 µm
particles
discharge channel
closed pores
coating thickness
pore band
interface
AM50
b)
10 µm
discharge channel
closed pores
pore band
coating thickness
interface
AM50
c)
10 µm
particles
closed pores
coating thickness
interface
AM50
d)
10 µm

3

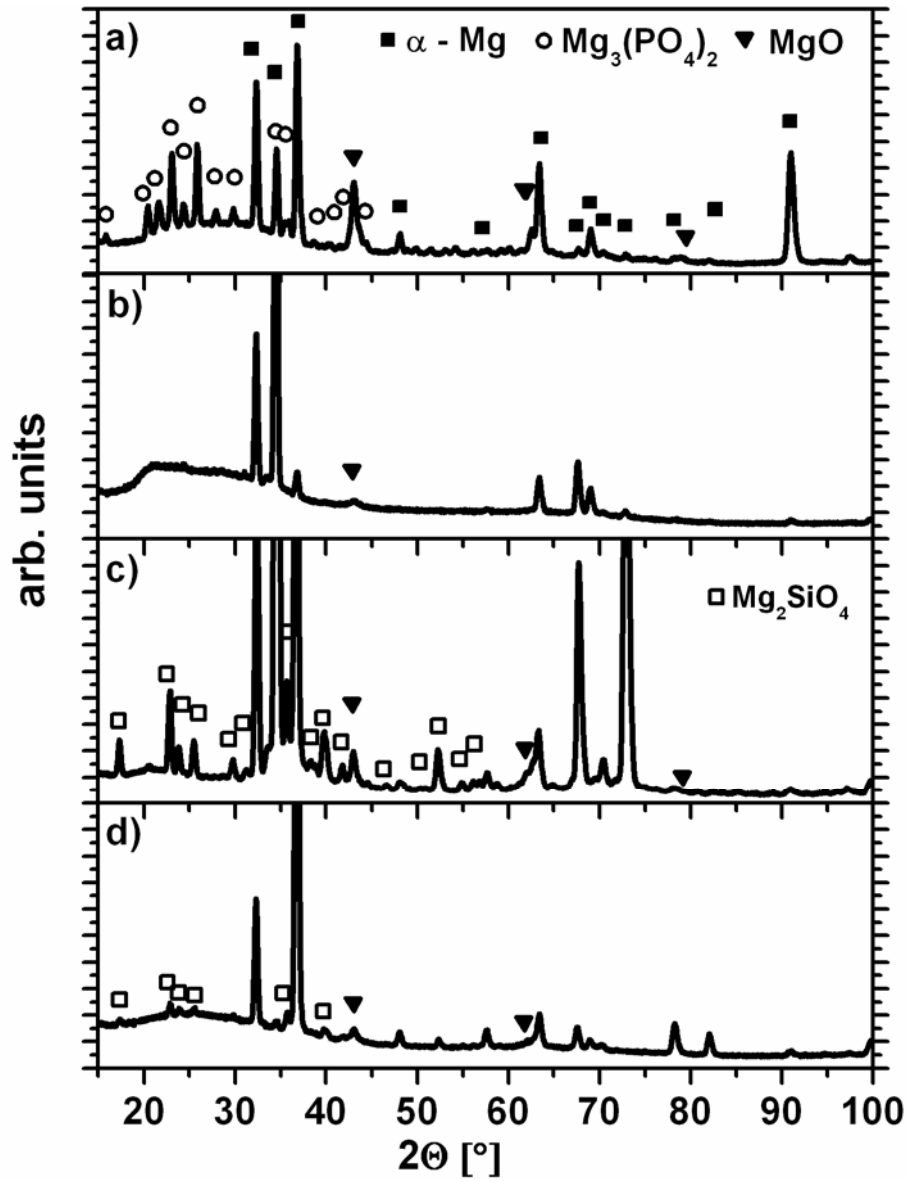
a)
α - Mg
Mg3(PO4)2
MgO
b)
c)
Mg2SiO4
d)
arb. units
20
30
40
50
60
70
80
90
100
2Θ [°]

4

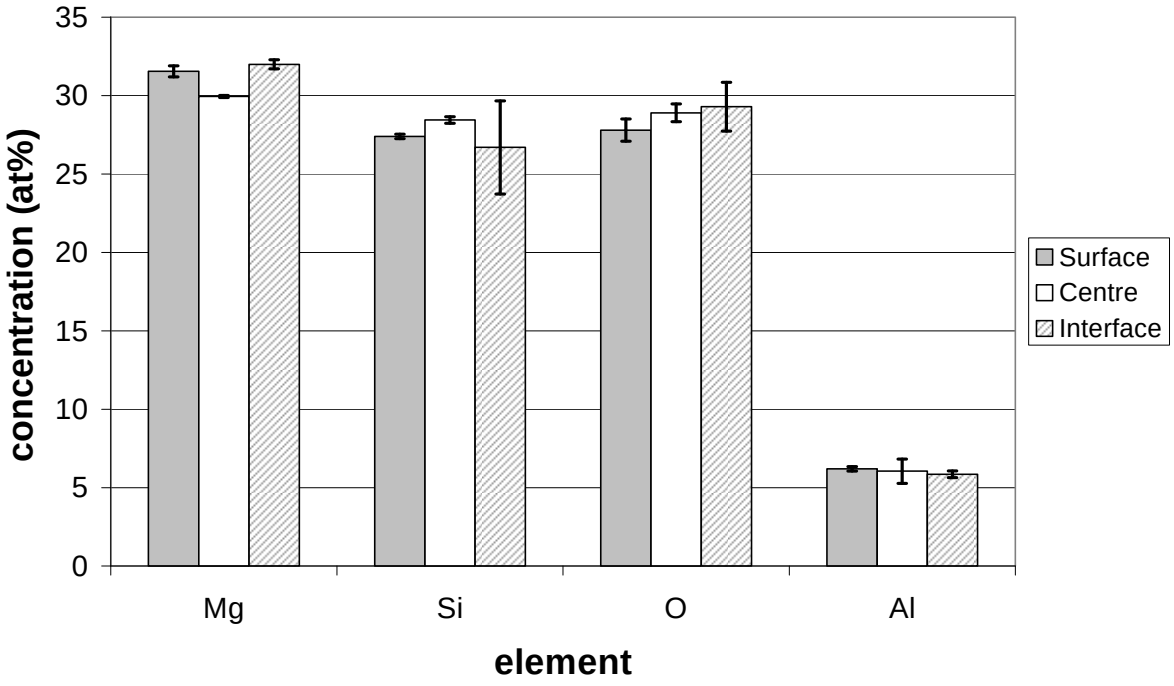
35
30
25
20
15
10
5
0
concentration (at%)
Mg
Si
O
Al
element
Surface
Centre
Interface

a)

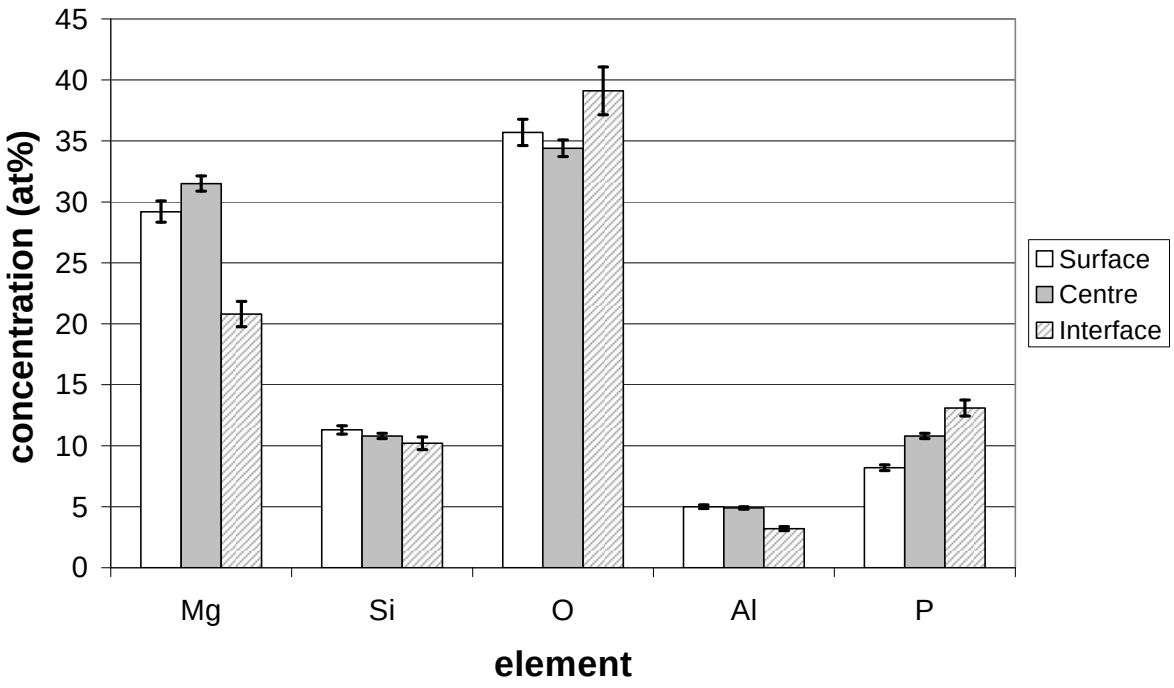
45
40
35
30
25
20
15
10
5
0
concentration (at%)
Mg
Si
O
Al
P
element
Surface
Centre
Interface

b)

5

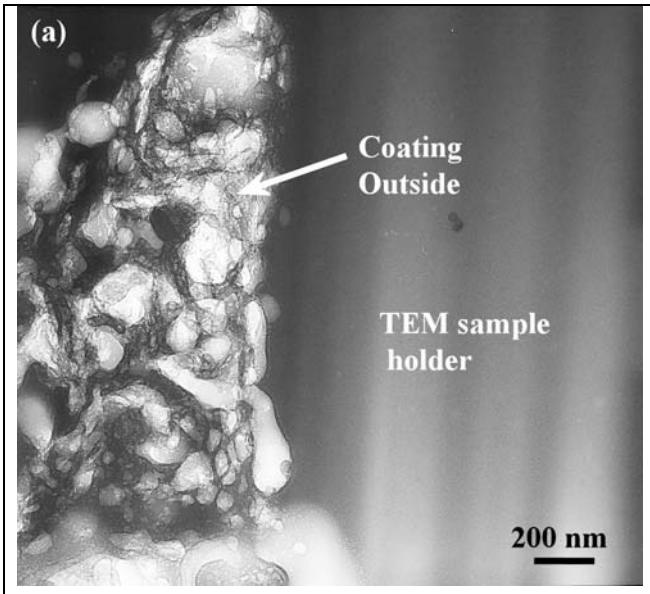
(a)
Coating
Outside
TEM sample
holder
200 nm

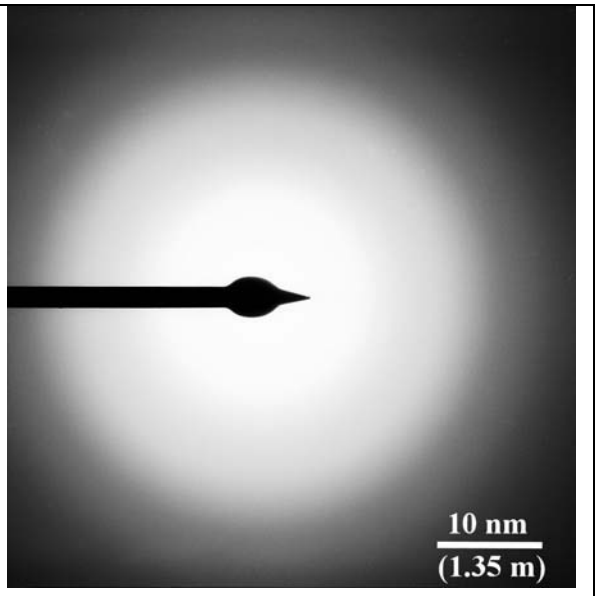
10 nm
(1.35 m)

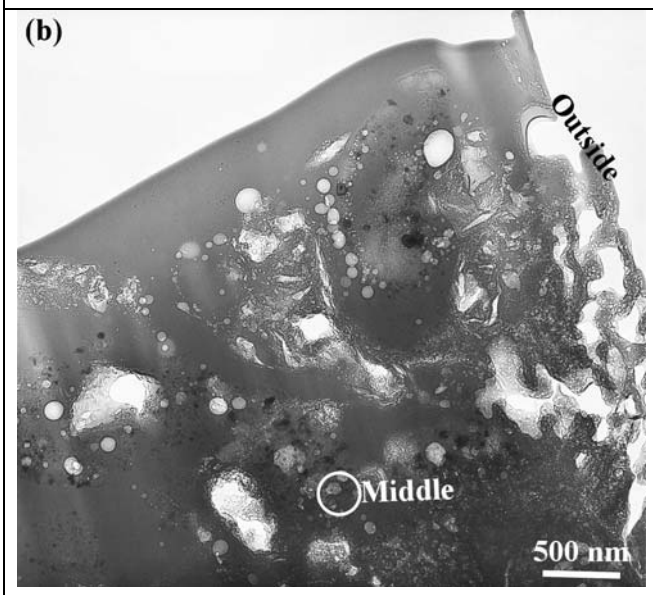
(b)
Outside
Middle
500 nm

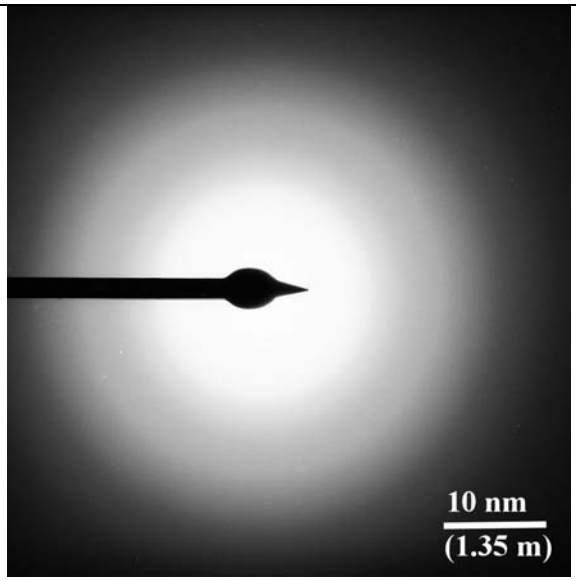
10 nm
(1.35 m)

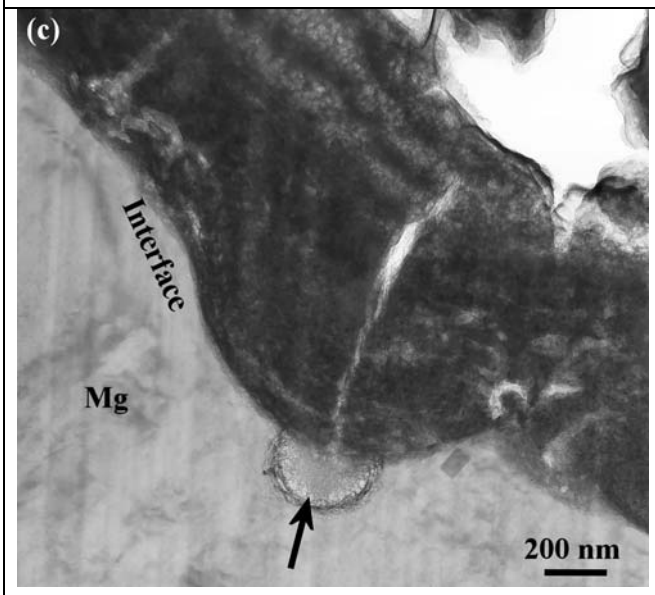
(c)
Interface
Mg
200 nm

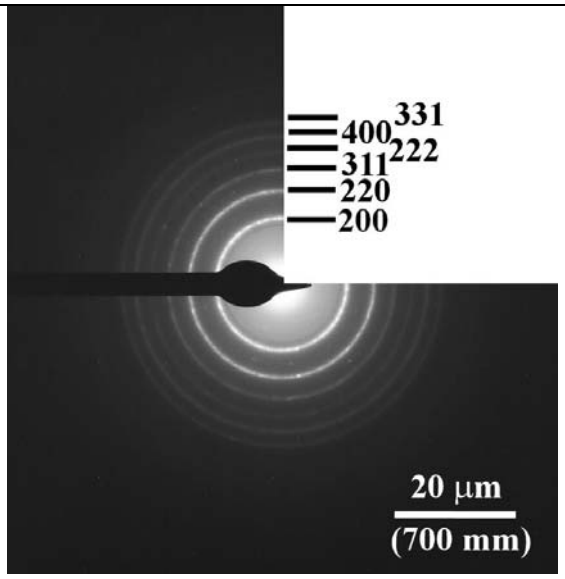
331
400
222
311
220
200
20 μm
(700 mm)

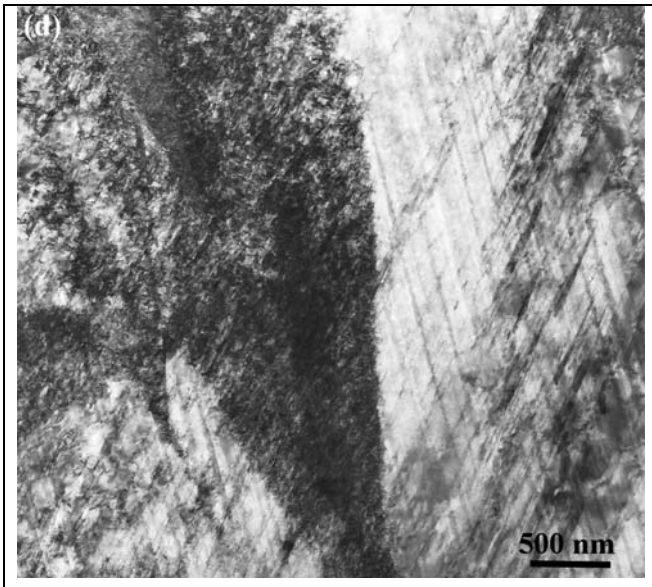
(d)
500 nm

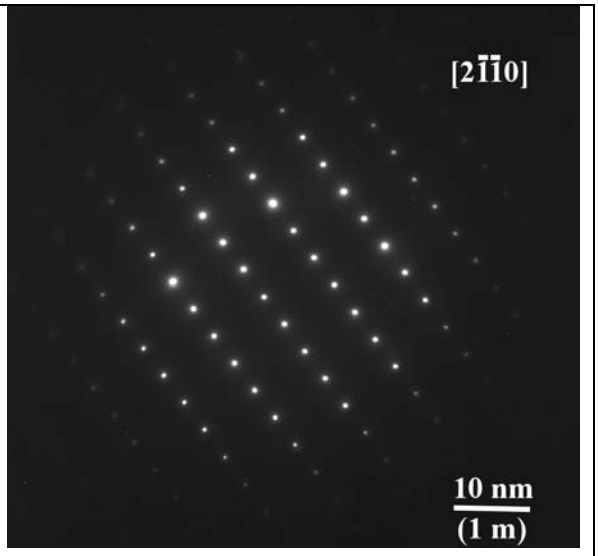
[2$\bar{1}\bar{1}$0]
10 nm
(1 m)